Capillary-mediated solid-liquid energy fields: their detection with phase-field method

IOP Conf. Series: Materials Science and Engineering **529** (2019) 012027 doi:10.1088/1757-899X/529/1/012027

Capillary-mediated solid-liquid energy fields: their detection with phase-field method

M Glicksman[1] and K Ankit[2]

[1] Florida Institute of Technology, 150 West University Blvd., Melbourne, FL 32901-6975, United States

[2] School for Engineering of Matter, Transport and Energy, Arizona State University, 551 E. Tyler Mall, ERC 265, Tempe, AZ 85287, United States

E-mail: [1]mglicksman@fit.edu, [2]kumar.ankit@asu.edu

Abstract. Observations of melting crystallites in microgravity showed unusual shape changes as melting proceeded toward extinction. When re-analyzed in 2011, shape evolution data showed needle-like crystallites becoming spheroids as they melted toward extinction, suggesting that some type of capillary phenomenon at solid-liquid interfaces was responsible for an energy release capable of spherodising particles on melting, and stimulating pattern formation during unstable crystal growth. The presence of these previously undetected energy fields was recently uncovered using phase-field simulations that employ an entropy density functional. Simulations allow measurement of interfacial energy distributions on equilibrated solid-liquid interfaces configured as *stationary* grain boundary grooves (GBGs). Interfacial energy source fields—related to gradients in the Gibbs-Thomson temperature—entail persistent cooling along GBG profiles, a new result that fully confirms earlier predictions based on sharp-interface thermodynamics. This study also provides new insights to improve microstructure control at reduced scales by explaining the thermodynamic fields responsible for pattern formation in castings.

1. Introduction

Solidification microstructures remain subjects of importance, as they affect the mechanical and chemical properties of primary metals, cast alloys, solder joints, and fusion welds. The origins of complex pattern formation in general [1, 2], including those observed throughout nature, such as snow flakes and crystalline minerals, remain as scientific issues with important technological applications. To achieve better control of microstructure formation in materials one must determine: 1) If pattern-forming "instructions" are somehow encoded on solid-liquid interfaces? If so, 2) Do these instructions devolve from some deterministic thermodynamic mechanism, or are they imposed extrinsically by noise and other random disturbances?

2. Grain Boundary Grooves

Grain boundary grooves (GBGs) are naturally occurring crystalline microstructures found along polycrystalline solid-liquid interfaces. GBGs affect interfacial dynamic behavior by reducing an interface's morphological stability through enhanced local heat and solute rejection into the melt. Their interactions with both stationary and moving solid-liquid interfaces were first reported experimentally in the late 1960s using hot-stage optical and electron microscopy.

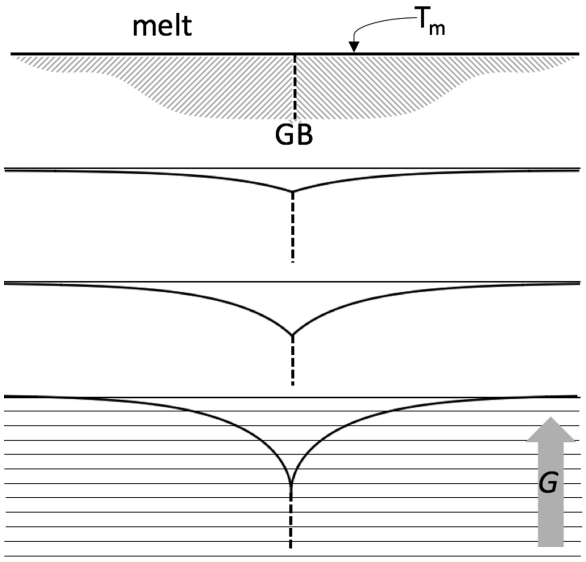

Figure 1. Sequence of virtual work steps to equilibrate an isolated GBG with a small dihedral angle. **Top**: Initial state, grain boundary (GB) intersects a flat solid-liquid interface. This interface locates the melting point isotherm, $T = T_m$. **Mid-panels**: Intermediate states, where the interface curves and lengthens, while the grain boundary shortens and the triple junction is drawn downward. **Bottom**: Final state, consisting of undercooled melt within the cusp depression in a vertical, constant temperature gradient, G, suggested by the stack of equally spaced isotherms.

Early studies on dilute alloys demonstrated that persistent defects, including GBGs, initiate morphological instabilities that stimulate complex patterns on solid-liquid interfaces [3, 4, 5]. Recently, dynamic effects induced by GBGs on solid-liquid interfaces in alloys were probed with phase-field simulation to follow morphological changes associated with interfacial instability [6].

2.1. Variational GBGs

The equilibrium profile for an isolated GBG, separating phases with equal thermal conductivity, was solved using variational calculus by Bolling and Tiller [7]. The profile, $\mu(\eta;\Psi)$, for a mirror-symmetric variational GBG, between phases of equal thermal conductivity, with dihedral angle, $\Psi \in [0,\pi)$, is described by the following pair of equations, plotted in figure 2 for $\Psi = 0$,

$$\begin{aligned}
\mu(\eta;\Psi) &= -\frac{1}{2}\left[\ln\left(\frac{\sqrt{1-\eta^2}-1}{\eta}\right) - \ln\left(\cot\frac{3\pi+\Psi}{8}\right)\right] - \sqrt{1-\eta^2} + \sin\left(\frac{\pi+\Psi}{4}\right), \quad \mu \geq 0 \\
\mu(\eta;\Psi) &= +\frac{1}{2}\left[\ln\left(\frac{\sqrt{1-\eta^2}-1}{\eta}\right) - \ln\left(\tan\frac{\pi-\Psi}{8}\right)\right] + \sqrt{1-\eta^2} - \cos\left(\frac{\pi-\Psi}{4}\right), \quad \mu \leq 0 \\
&\qquad\qquad \eta \in [\eta^\star(\Psi), 0).
\end{aligned} \tag{1}$$

The leading minus sign in equation (1) denotes a GBG's right-side profile, $0 \leq \mu \leq \infty$, whereas the leading plus sign denotes its left-side profile, $-\infty \leq \mu \leq 0$. Also, the limited range of negative η-values allowed for equations (1) is $\eta^\star(\Psi) \leq \eta < 0$, where $\eta^\star(\Psi) = -\sqrt{\frac{1}{2}(1-\cos\frac{\pi-\Psi}{2})}$.

The system's thermo-capillary length, $\Lambda \equiv \sqrt{\frac{\gamma_{s\ell}\ \Omega}{G\Delta S_f}}$, determines the equilibrated (physical) size for variational GBGs derived from calculus. The materials constants defining Λ are $\gamma_{s\ell}$ [J/m^2], the solid-liquid interfacial energy density; Ω [m^3/mole] the molar volume of both phases; and ΔS_f [J/mole·K], the solid-liquid system's molar entropy change on melting. G, however, is the system parameter setting the magnitude of the temperature gradient and the GBG's size.

2.2. Equilibria on curved solid-liquid interfaces

The scaling law implicit in the definition of Λ also defines the appropriate temperature interval needed to non-dimensionalize the Gibbs-Thomson equilibrium interface temperature into a useful

steady-state thermo-potential distribution along curved solid-liquid interfaces in the presence of a constant temperature gradient. The Gibbs-Thomson temperature distribution provides several important thermodynamic effects, largely ignored to date, that are intimately related to pattern formation during solidification.

At fixed pressure in the melt, the Gibbs-Thomson temperature distribution connects interface curvature, $\kappa(y(x))$ [m^{-1}], of a solid-liquid interface with its local equilibrium temperature, or chemical potential. For the case of a stationary GBG separating pure solid and liquid with equal thermal conductivities, held in a uniform temperature gradient, G, the interface temperature, $T_{int}(y(x))$ [K], decreases *linearly* with depth coordinate, y. Local undercooling within the melt cusp, viz., $(T_{int}(y(x)) - T_m)$ [K], increases linearly as $G \times y$ [K]. Thus, for equilibrated GBGs, portrayed in figures 1 and 2, their undercooling [K] and interface curvatures [m^{-1}] remain proportionate per the well-known Gibbs-Thomson relationship,

$$T_{int}(y(x)) - T_m = -\left(\frac{\gamma_{s\ell}\Omega}{\Delta S_f}\right)\kappa(y(x)). \tag{2}$$

Melt undercooling [K] can be transformed to a non-dimensional thermo-potential, ϑ, by dividing equation (2) by a suitable temperature interval. The temperature interval characteristic of a GBG is $2G \times \Lambda$ [K] that approximates the maximum undercooling developed at a GBG's triple junction. This choice defines a dimensionless thermo-potential, $\vartheta(y(x))$, namely,

$$\vartheta(y(x)) \equiv \frac{(T_{int}(y(x)) - T_m)}{2G\Lambda} = -\left(\frac{\gamma_{s\ell}\Omega}{2G\Lambda\Delta S_f}\right)\kappa(y(x)). \tag{3}$$

A non-dimensional curvature, $\hat{\kappa}$, defined consistently with the system's capillary length, Λ, is $\hat{\kappa}(\eta(\mu)) \equiv \kappa(y(x)) \times 2\Lambda$. Introducing that curvature into the foregoing Gibbs-Thomson relation, equation (3), allows a GBG's thermo-potential to be expressed in non-dimensional (μ, η) coordinates as,

$$\vartheta(\eta(\mu)) = -\left(\frac{\gamma_{s\ell}\Omega}{2G\Lambda\Delta S_f}\right)\hat{\kappa}(\eta(\mu)) \times \left(\frac{1}{2\Lambda}\right). \tag{4}$$

Gathering all the material and system constants that appear in equation (4), and inserting the lumped parameters that define the GBG's length scale Λ, shows that $\frac{\gamma_{s\ell}\Omega}{G\Lambda^2\Delta S_f} = 1$. Thus, judicious selections of the length and temperature scales allow the Gibbs-Thomson temperature for a variational GBG to assume the simple form, $\vartheta(\eta(\mu)) = -\frac{1}{4}\hat{\kappa}(\eta(\mu))$. The in-plane curvature distribution for any variational groove profile, equations (1), can be evaluated using the well known differential calculus formula [8], $\hat{\kappa}(\mu(\eta)) \equiv \frac{d^2\eta/d\mu^2}{(1+(d\eta/d\mu)^2)^{2/3}} = -4\eta$, $(0 \geq \eta \geq \eta^\star(\Psi))$. Note, that under the constrained equilibrium provided by the applied temperature gradient,

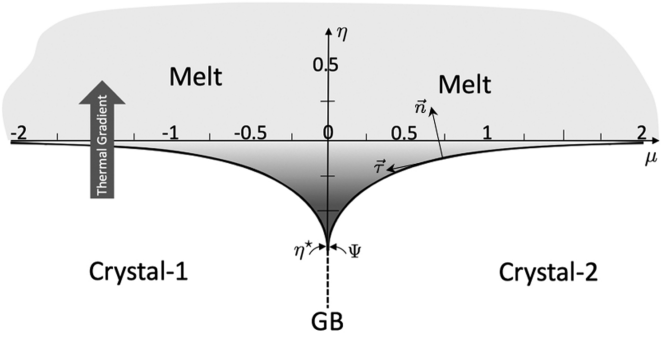

Figure 2. Variational GBG profile, $\mu(\eta; \Psi)$, plotted with equation (1), and its scaled coordinates $\mu = x/2\Lambda, \eta = y/2\Lambda$. The interfacial slope and curvature both vanish as $\mu \to \pm\infty$. The length scale, Λ, depends inversely on the magnitude of the gradient, G, in the $+\eta$ direction. This gradient constrains the entire profile to lie between the μ-axis and the groove's triple junction at $\mu = 0$, $\eta = \eta^\star(\Psi)$.

G, the interface curvature and the thermo-potential both approach zero as $\eta \to 0$, and $\mu \to \pm\infty$. Moreover, when the curvature, $\hat{\kappa} = -4\eta$, is substituted into the thermo-potential, $\vartheta(\eta(\mu)) = -\frac{1}{4}\hat{\kappa}(\eta(\mu))$, one finds that this interface thermo-potential equals the value of the GBG's depth coordinate, η,

$$\vartheta(\eta(\mu)) = \eta(\mu), \quad (0 \geq \eta \geq \eta^{\star}(\Psi)). \tag{5}$$

As shown next, this linear distribution of scalar Gibbs-Thomson thermo-potentials along the depth coordinate, η, implies much more than merely matching chemical potentials at thermodynamic equilibrium. They also provide a vector gradient field along the interface.

2.3. Interface gradients and fluxes

A directional gradient field from the Gibbs-Thomson scalar thermo-potential distribution, equation (5), exists tangentially along the solid-liquid interface. This field may be calculated from the following vector operational sequence,

$$\vec{\nabla}_{\tau}[\vartheta(\eta(\mu))] = \frac{d}{d\eta}[\vartheta(\eta(\mu))]\left(\frac{d\eta}{d\hat{s}}\right)\vec{\tau}, \quad \eta(\mu) \in \mathbb{R}^2 \tag{6}$$

where $\hat{s}$ is the GBG's dimensionless arc length of its profile, scaled similarly by twice the thermo-capillary length, 2Λ. The Frenet frame vector in equation (6), $\vec{\tau}$, is the unit tangent along the interface. The arc-length derivatives, $d\eta/d\hat{s}$, on the left and right profiles are, respectively,

$$d\eta/d\hat{s} = \pm 1/\sqrt{1 + (d\mu/d\eta)^2} = \mp 2\eta\sqrt{1-\eta^2}, \quad (\eta < 0). \tag{7}$$

When equations (5) and (7) are substituted into the chain rule, equation (6), one obtains the explicit expressions for the *vector* arc-length gradients of the Gibbs-Thomson thermo-potential along the right and left GBG profiles, respectively,

$$\vec{\nabla}_{\tau}[\vartheta(\mu(\eta);\Psi)] = \pm 2\eta\sqrt{1-\eta^2}\cdot\vec{\tau}, \ (0 \geq \eta \geq \eta^{\star}(\Psi)), \tag{8}$$

The presence of vector gradients in the thermo-potential requires an *irreversible* interfacial response according to Fourier's law of heat conduction in 2-D. Specifically, an energy flux [W/m] is spontaneously stimulated along the solid-liquid interface in directions opposite to those of the interface's local thermo-potential gradient vectors, equations (8). Application of Fourier's law introduces an interfacial thermal conductivity, k_{int} [W/K]—the value for which is the *bulk* thermal conductivity [W/m-K] of the solid and liquid phases multiplied by a thickness [m], of the order of the effective width of the solid-liquid interface. This interfacial transport number is well defined and has been analyzed theoretically [9]. Unfortunately, estimates for its values have received little attention from experimental heat transfer research for solid-liquid systems. Nevertheless, the dimensional forms of these tangentially stimulated Gibbs-Thomson energy fluxes on the right and left GBG profiles may be expressed as,

$$\vec{\phi}_{\tau}(y(x);\Psi) = \mp\left(\frac{2Gk_{int}}{\Lambda}\right) y\sqrt{1-\frac{y^2}{4\Lambda^2}}\cdot\vec{\tau} \quad (y<0) \quad [\mathrm{W/m}]. \tag{9}$$

The non-dimensional form of this capillary-mediated heat flux, $\hat{\Phi}(\eta(\mu);\Psi)$, is found by dividing equations (9) by the lumped constant Gk_{int} [W/m], to yield expressions identical to equations (8) for the tangential gradients, but of opposite sign.

$$\hat{\Phi}(\eta(\mu);\Psi) = \mp 2\eta\sqrt{1-\eta^2}\cdot\vec{\tau}. \tag{10}$$

2.4. Capillary bias fields

The presence of tangential interface fluxes, equations (10), has several interesting inferences. First, as *tangential* energy fluxes, these capillary-mediated energy streams, caused by gradients in the distribution of the Gibbs-Thomson thermo-potentials along the solid-liquid interface, are not directly interactive with the interface. The reason for their indirect interaction is that the energy balance controlling interface speed responds only to fluxes directed *normal* to the interface, not tangentially. Second, the quasi-static thermal fields, $T(\mu,\eta)_i$, $i{=}s,\ell$, within the bulk phases forming a GBG, which are established by the applied temperature gradient, G, each obey Laplace's equation. Laplace temperature distributions *within* the bulk phases are "harmonic" fields, which preclude divergence of their heat fluxes. This harmonic restriction, however, does not apply to the capillary-mediated fluxes moving along the interface itself, i.e., heat flowing *between* the phases! This peculiar and, to date, unnoticed distinction is of critical importance to understanding how perturbing energy fields arise from capillarity and modify the local speed of solid-liquid interfaces. Tangential fluxes obey Poisson's equation, and are divergent, i.e., they result in small releases or removals of energy along the interface, which act as Poisson sources. This qualitative difference among the system's interacting thermal fields accounts for capillary-induced contributions to the local energy budget of curved solid-liquid interfaces, both moving and stationary.

Specifically, capillary-mediated thermo-potential gradients along interfaces obey the following Poisson equation [10],

$$\nabla_\tau^2 \vartheta(\mu(\eta);\Psi) = \mathfrak{B}(\eta(\mu)), \tag{11}$$

where $\mathfrak{B}(\eta(\mu))$, the bias field, acts as the interfacial source/sink function.

Equation (11) shows that bias fields, mathematically, are also the *surface Laplacian* of the Gibbs-Thomson potential, or equivalently, they equal (minus) the arc-length divergence of the capillary-mediated tangential vector flux, $-\vec{\nabla}_\tau \cdot [\hat{\Phi}(\eta(\mu);\Psi)]$. The key issue to be resolved in this paper is to demonstrate how interfaces, such as stationary GBGs, also support 'active' Poisson sources or sinks that provide intrinsic interface perturbations. Stationary microstructures, open to energy exchange, also interact with their own Poisson bias fields and provide an unique opportunity to generate a *persistent perturbations* once the microstructure and its source field are equilibrated. This occurs for GBGs without suffering the additional complications of complex pattern generation or other significant microstructure changes associated with morphologically unstable moving solid-liquid interfaces.

The Poisson source, or bias field, for a grain boundary groove may be calculated analytically from its Gibbs-Thomson potential distribution by twice arc-length differentiating equation (5). This is accomplished applying the following nested set of elementary operations in $\mathbb{R}^2$,

$$\nabla_\tau^2 \vartheta(\eta(\mu)) = \frac{d}{d\eta}\left[\frac{d}{d\eta}[\vartheta(\eta(\mu);\Psi)]\left(\frac{d\eta}{d\hat{s}}\right)\vec{\tau}\right]\cdot\left(\frac{d\eta}{d\hat{s}}\right)\vec{\tau}. \tag{12}$$

The operational sequence shown in equation (12) defines the surface Laplacian of the Gibbs-Thomson equilibrium thermo-potential specified in equation (5). The bias field, $\mathfrak{B}(\eta(\mu))$, which in 2-D is $d^2\vartheta/d\hat{s}^2$, describes the dimensionless distribution of rates at which divergent capillary-mediated fluxes steadily remove thermal energy along a GBG's solid-liquid interface. The result for any GBG is the (negative) cubic distribution of energy rates,

$$\mathfrak{B}(\eta(\mu);\Psi) = 16\eta(1-2\eta^2),\ (0 \geq \eta \geq \eta^\star(\Psi)). \tag{13}$$

Equation (13), provides a close approximation to the actual Poisson perturbation field resident on a fully equilibrated GBG. This occurs, somewhat fortuitously, because the shape modifications of a stationary GBG induced by capillary perturbation fields are extremely small, so variational

GBG profiles accurately portray the actual curvature distributions along an equilibrated grain boundary groove supporting a basis field.

Equation (13), plotted as smooth curves in figure 3, shows that the bias field along any stationary GBG is everywhere negative and steady state. Negative bias fields cause cooling, i.e., energy removal, and correspond to positive vector divergences of the tangential capillary-mediated flux. Thus, the tangential heat flux, by virtue of its (positive) divergence, steadily *removes* energy from a GBG's solid-liquid interface *everywhere*, especially deep within the cusp. This self-induced energy removal cools the interface slightly, causing its curvature to increase (responding to the Gibbs-Thomson effect), and spontaneously "biases" the interface toward local equilibrium, as predicted by the Le Châteliér-Braun effect.

Bias fields on *moving* solid-liquid interfaces can behave in more complex ways, and may heat and cool different interfacial regions. Added or diminished energy rates both affect a moving interface's local energy budget. The interface speed responds immediately to conserve energy at all points by slowing or accelerating latent heat production, respectively. In this sense, the capillary field biases or modulates the motion of a moving interface, and can stimulate complex microstructure pattern development if the interface is morphologically unstable.

3. Phase-field Simulations and Results

We formulated an entropy density functional, $\mathcal{S}(e,\boldsymbol{\phi})=\int_V(s(e,\boldsymbol{\phi})-(\epsilon a(\boldsymbol{\phi},\nabla\boldsymbol{\phi})+\frac{1}{\epsilon}w(\boldsymbol{\phi})))dV$, for phase-field computations of thermal grain boundary grooving, a model that ensures consistency with classical irreversible thermodynamics. The bulk entropy density, s, depends on the internal energy density, e, and phase indicator, $\boldsymbol{\phi} = (\phi_\alpha)_{\alpha=1}^{N}$, the latter being a vector of phase-field variables that lies in the $N-1$ dimensional plane. Two grains and their melt ($N = 3$) are the phases needed to model a GBG microstructure. $a\,(\boldsymbol{\phi},\nabla\boldsymbol{\phi})$ and $w\,(\boldsymbol{\phi})$ represent the gradient and obstacle potential type energy density, respectively; ϵ is a small length-scale parameter related to the thickness of the diffuse interfaces; and V represents the domain volume. Details of this simulation method are available in [11, 12]. Interface residual measurements to detect bias fields are fully disclosed in [13, 14].

Phase-field simulations, as very briefly described here, were used to probe stationary GBGs, which, upon equilibration in an applied linear temperature gradient, spontaneously develop interfacial Poisson sources (capillary-mediated perturbation fields). The opportunity to equilibrate a stationary microstructure, and then 'uncover' and measure its resident bias-field, presents a novel extension of phase-field simulation. Importantly. it permits independent verification of the existence of steady-state interfacial bias-fields.

Precision interface potential measurements conducted in our study reached levels of detection well below that which could possibly be accomplished experimentally, which allowed successful extraction of small "residuals" caused by non-linear interactions between the interface and its capillary-mediated fields. Residuals were the differences of the measure isoline potentials and the linear potentials imposed by the applied constant temperature gradient, G.

In order to obtain residuals data from simulations, GBG microstructures must achieve equilibrated stationary configurations in an applied temperature gradient, so that their input shapes become slightly modified by interaction with their self-generated capillary bias fields.

4. Conclusions

(i) Steady-state distributions of interfacial GBG thermo-potentials are the sum of the applied gradient, in which the GBGs are equilibrated, plus small non-linear contributions that arise from autogenous interfacial energy sources. The key issue divulged in this study that led to independent verification of these higher-order thermodynamic fields was spontaneous energy absorption from GBG interfaces. The energy removal occurred because tangential

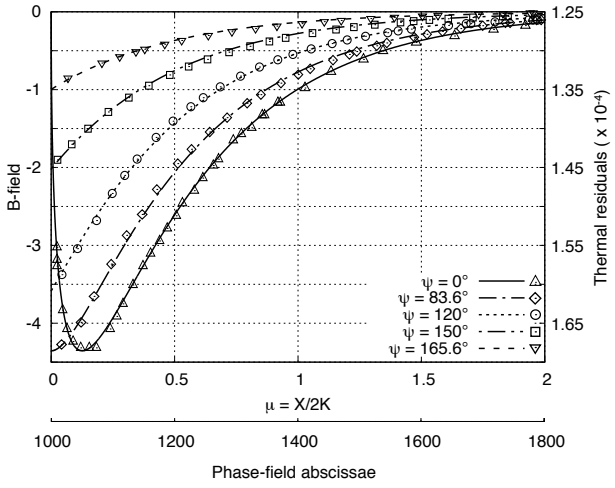

Figure 3. Comparison of phase-field residuals (data) from simulated GBGs equilibrated at steady-state with predicted $\mathfrak{B}$-fields (curves) obtained from sharp-interface theory. Residuals data measured on simulated diffuse interfaces agree well with theoretical estimates based on sharp interface thermodynamics. These results show that capillary-mediated bias fields are present at equilibrium on equilibrated GBG interfaces.

gradients and heat fluxes of the Gibbs-Thomson thermo-potential are divergent vector fields. Positive divergence of this capillary-mediated tangential energy flux causes energy loss at the solid-liquid interface, i.e., cooling, which results in small decreases of the Gibbs-Thomson thermo-potential, and consequent small increases in the interface curvature required by the system's shift toward local equilibrium.

(ii) The distribution of residuals is the result of—and, as explained in [13, 14], proportionate to—the capillary source distribution affecting the local thermal balance. Residuals are plotted as the data points in figure 3, all of which closely mimic the distributions of cooling perturbations, $\mathfrak{B}$-fields, plotted as smooth curves predicted from sharp-interface thermodynamics and field theory for variational GBGs.

(iii) When simulated, GBG profiles achieve thermal equilibration, and we observed no significant changes from their analytical shapes. We detected only "cooler" interfaces, i.e., by detecting negative residuals of the potential, caused by energy removal through the GBG's (negative) capillary bias field, equation (13). Again, the quantitative agreement demonstrated in figure 3 between residuals, i.e., non-linear potential depressions, and their calculated causal cooling rates, $\mathfrak{B}(\mu(\eta))$, reflects the predicted proportionality expected between interfacial cooling rates and measured decreases in thermo-potential.

(iv) These data provide indirect, but firm, support for our previous claim that it is capillary-mediated interfacial energy fields, previously unrecognized as required for *omnimetric* interfacial energy balances, that are causal for microstructure formation during solidification. Future microstructure control strategies during casting should recognize their presence for further improvement and control of microstructure patterns.

Acknowledgments
Author MG thanks the Allen S. Henry endowed Chair of Engineering, which provided support for this research at the Florida Institute of Technology, Melbourne, Florida. Both authors acknowledge financial support from the National Aeronautics and Space Administration (NASA) through Grant Number 80NSSC18K1440.

References

[1] Thompson D 1948 *On Growth and Form,* 2nd *Edn.* (Cambridge, UK: Cambridge University Press)
[2] Kassner K 1996 *Pattern Formation in Diffusion-Limited Crystal Growth* Directions In Condensed Matter Physics (Singapore: World Scientific Publishing Co. Pte. Ltd.)

[3] Morris L and Winegard W 1969 *J. Cryst. Growth* **5** 361–375
[4] Schaefer R and Glicksman M 1970 *Met. Trans.* **1** 1973–1978
[5] Sharp R and Hellawell A 1970 *J. Cryst. Growth* **6** 334–340
[6] Yeh S, Chen C and Lan C 2011 *J. Cryst. Growth* **324** 296–303
[7] Bolling G and Tiller W 1960 *J. Appl. Phys.* **31** 1345
[8] Kells L 1946 *Calculus* 7$^{\text{th}}$ Ed. (New York: Prentice-Hall, Inc.)
[9] Gurtin M 1988 *Archive for Rational Mechanics and Analysis* **104** 195–221
[10] Glicksman M 2016 *J. Cryst. Growth* **450** 119–139
[11] Garcke H, Nestler B and Stinner B 2004 *SIAM J. Appl. Math.* **64** 775
[12] Nestler B, Garcke H and Stinner B 2005 *Phys. Rev. E* **71** 041609
[13] Glicksman M and Ankit K 2017 *Metals* **7**(12) 547
[14] Glicksman M and Ankit K 2018 *J. Mater. Sci.* **53** 10955–10978